Modeling Hydrogen Transport in BABY

by

Colin Weaver

Submitted to the Department of Mechanical Engineering
in partial fulfillment of the requirements for the degree of

BACHELOR OF SCIENCE IN MECHANICAL ENGINEERING

at the

MASSACHUSETTS INSTITUTE OF TECHNOLOGY

May 2024

Authored by: Colin Weaver
Department of Mechanichal Engineering
May 10, 2024

Certified by: Sara E. Ferry
Department of Nuclear Science and Engineering, Thesis Supervisor

Accepted by: Kenneth Kamrin
Associate Professor of Mechanical Engineering
Undergraduate Officer, Department of Mechanical Engineering

Modeling Hydrogen Transport in BABY

by

Colin Weaver

Submitted to the Department of Mechanical Engineering
on May 10, 2024 in partial fulfillment of the requirements for the degree of

BACHELOR OF SCIENCE IN MECHANICAL ENGINEERING

ABSTRACT

Fusion energy stands as a beacon of hope in the realm of sustainable power generation, offering the potential to meet global energy demands without adverse environmental impacts. However, fusion power is not yet commercially viable, and significant research is still needed to develop the technologies necessary to make it a reality. Central to the realization of practical fusion reactors is the efficient management of tritium, a scarce and radioactive isotope that serves as the fuel in a deuterium-tritium fusion reaction. The liquid immersion blanket concept, pioneered by endeavors like Commonwealth Fusion Systems, represents a significant stride towards addressing the challenges of tritium breeding and extraction. At the forefront of this endeavor lies the LIBRA Experiment, the goal of which is to better understand tritium breeding, containment, and extraction under a fusion-like neutron spectra, and BABY, a scaled-down iteration of the LIBRA Experiment designed to serve as a stepping stone to the full LIBRA Experiment. BABY serves as a testbed for evaluating Tritium extraction mechanisms and assessing the feasibility of achieving self-sufficiency in fuel production within a fusion power plant environment. In this context, understanding hydrogen transport phenomena within the BABY system emerges as a crucial aspect of optimizing tritium extraction and ensuring tritium self-sufficiency. By employing advanced modeling techniques simulating fluid flow and heat transfer to inform tritium transport simulations in FESTIM, this thesis endeavors to elucidate the intricacies of hydrogen migration mechanisms, diffusion rates, and their impact on tritium dynamics within the molten salt environment of BABY. Steady state simulations of bulk tritium transport coefficients provide results for the range of tritium transport coefficients for BABY, while transient simulations provide insight into the complex dynamics surrounding tritium transport through the various surfaces of BABY. The findings of this study hold profound implications for the fusion energy landscape, offering valuable insights that can inform the design and operation of future fusion reactors utilizing liquid immersion blankets. By elucidating the factors governing hydrogen transport in BABY, this research aims to contribute to the overarching goal of achieving sustainable and efficient fusion energy production.

Thesis supervisor: Sara E. Ferry
Title: Department of Nuclear Science and Engineering

Acknowledgments

Thank you to Dr. Sara Ferry for your supervision on this thesis project, and for providing the amazing opportunity to do research on tritium transport in BABY. Being able to contribute to your group as well as work so closely with a project that has so much potential impact on the world has been such a blessing. Thank you also to Dr. Kevin Woller for the supervision under this tight-knit group.

A special thank you to Remi Delaporte-Mathurin for his day-to-day guidance on all of the small details of this research project. The research presented in this thesis would have been in no way possible without the many hours spent guiding and fine-tuning me and my research throughout this process. Also thank you to James Dark for your special guidance and support with modeling that helped push this project forward on multiple occasions.

Contents

List of Figures

List of Tables

Chapter 1

Background

1.1 Fusion: General Introduction

1.1.1 Thermonuclear Fusion

Thermonuclear fusion stands as a monumental feat of harnessing the power of the stars to meet terrestrial energy needs. At its core, fusion involves the fusion of light atomic nuclei, typically isotopes of hydrogen, to form heavier elements, releasing tremendous amounts of energy in the process.

In the context of thermonuclear fusion, the release of energy arises from the conversion of mass into energy during nuclear reactions. When light atomic nuclei, such as deuterium and tritium, fuse to form heavier elements, the total mass of the fused products is slightly less than the total mass of the original nuclei. This difference in mass, is converted into energy according to Eq. 1.1.

$$E = mc^2 \tag{1.1}$$

The concept of binding energy, which is the energy required to completely separate its constituent nucleons into free particles, makes very clear why light elements are so preferred for releasing energy from fusion. Fig. 1.1 depicts the binding energies of atoms. Smaller atoms, such as isotopes of hydrogen, have higher binding energies per nucleon compared to larger atoms. This means that a greater fraction of the mass of smaller atoms is converted into binding energy when they undergo fusion reactions. However, these reactions still require immense temperatures and pressures.

The primary fusion reaction of interest for practical energy generation involves the isotopes of hydrogen: deuterium (^{2}H) and tritium (^{3}H). The fusion of deuterium and tritium nuclei under conditions of high temperature and pressure yields helium (^{4}He) and a neutron, along with an enormous release of energy [2]:

$$^2\mathrm{H} +^3 \mathrm{H} \rightarrow^4 \mathrm{He} + n + 17.6\,\mathrm{MeV} \tag{1.2}$$

Magnetic confinement fusion, MCF, exemplified by devices like tokamaks and stellarators, employs magnetic fields to confine and heat the fusion fuel to the extreme temperatures required for fusion reactions to occur. At the core of a tokamak lies, the plasma, which is

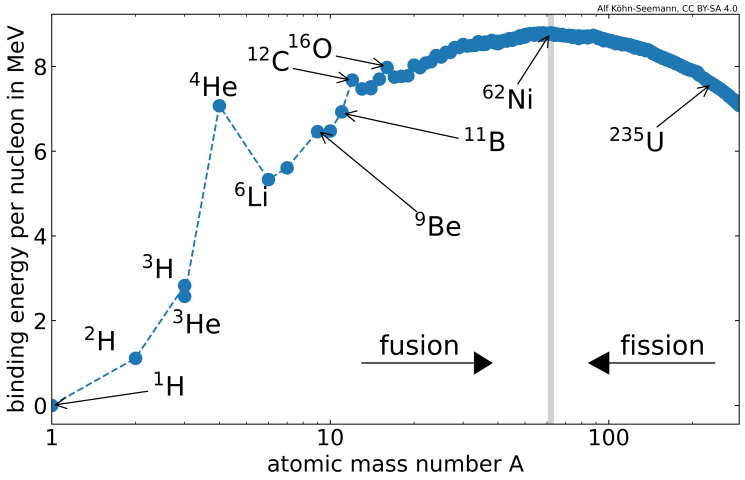

Figure 1.1: Illustration of binding energies per nucleon in MeV from [1]. Deuterium and tritium pictured in bottom left. Elements to the left of the grey line give off more energy in fusion than in fission.

the deuterium-tritium fuel heated to extreme temperatures, and surrounding the core are plasma facing components that must be able to withstand the extreme heat flux put off by the reactions happening in the plasma.

Central to the feasibility and viability of fusion energy is the challenge of achieving and sustaining the conditions necessary for fusion reactions to occur. This entails overcoming many formidable barriers, the most central of which to this paper is tritium breeding and extraction.

1.1.2 Tritium Availability Challenges

While hydrogen is the most abundant element in the universe, and deuterium, also called heavy water, can be found in large supply, tritium, the isotope of hydrogen containing one proton and two neutrons, can only be used to supply fusion power plants from the 30 kilograms worldwide [3]. This is a significant problem for the fusion industry considering ITER, like other prospective first fusion power plants that are projected to produce more power than the energy needed to sustain them will require 0.9 kilograms of tritium per year during its lifetime [4].

Tritium has a number of other downsides including hydrogen embrittlement [5], and health concerns since it is a hazardous, radioactive isotope. Tritium decays with a half life of 12.3 years [6] according to:

$$^{3}\mathrm{H} \rightarrow ^{3}\mathrm{He} + e^{-}(18.590\,\mathrm{keV}) \tag{1.3}$$

The scarce nature of the availability of tritium means that the first fusion power plants will have to produce their own tritium if they are to use it as fuel. To follow a 5 year power plant doubling cycle, which is typical of the energy industry, the amount of tritium produced by the reactor must be at least 1.15 times what goes in as fuel [7]. This number is referred to as the tritium breeding ratio (TBR). These factors further emphasize the need for a thorough

understanding of how tritium can move through a system for effective usage of the limited energy supply.

1.1.3 Tritium Challenges in Liquid Immersion Blankets

In recent years, the concept of a liquid immersion blanket (LIB) has emerged as a promising solution in breeding blanket designs. By surrounding the fusion plasma with a liquid blanket, comprised of molten salts or other suitable materials, these blankets serve multiple functions, including thermal management, radiation shielding, and tritium breeding. This technology shows great promise and is being implemented by Commonwealth Fusion Systems, CFS, one of the most promising leaders in creating a viable fusion power plant [8].

To achieve this, the neutrons from D-T fusion reactions can be utilized by components that contain lithium and surround the plasma to breed tritium. There are two possible reactions between lithium and neutrons:

$$^{6}\mathrm{Li} + n \rightarrow ^{3}\mathrm{H} + ^{4}\mathrm{He} + 4.8\,\mathrm{MeV} \tag{1.4}$$

$$^{7}\mathrm{Li} + n \rightarrow ^{3}\mathrm{H} + ^{4}\mathrm{He} + n - 2.5\,\mathrm{MeV} \tag{1.5}$$

The component surrounding the plasma reactions that contains lithium and acts as a way of producing tritium is often referred to as a breeding blanket, and building effective breeding blankets is crucial for being able to extract the new tritium and breeding enough tritium to support a growing fusion industry.

CFS proposes a LIB design in their fusion power plant, ARC, that utilizes FLiBe, short for Lithium Fluoride (LiF) and Beryllium Fluoride (BeF2), as a coolant and neutron moderator in the LIB. Because FLiBe is a liquid and carries such a crucial role in extracting heat and breeding tritium, understanding how tritium moves through a FLiBe LIB is of the utmost importance to CFS.

1.1.4 Tritium Transport Methods and Challenges

Diffusive hydrogen transport involves the movement of hydrogen atoms or molecules through a medium, driven by concentration gradients or other thermodynamic forces. Fig. 1.2 depicts the many mechanisms driving diffusion of hydrogen through materials including interstitial diffusion, implantation, and trapping.

This process can be generally described by Fick's second law of diffusion which describes how the concentration in a medium evolves with time, driven by the concentration gradient of hydrogen in the material:

$$\frac{\partial c}{\partial t} = \nabla \cdot (D \nabla c) \tag{1.6}$$

where:

- c represents the concentration
- t is time

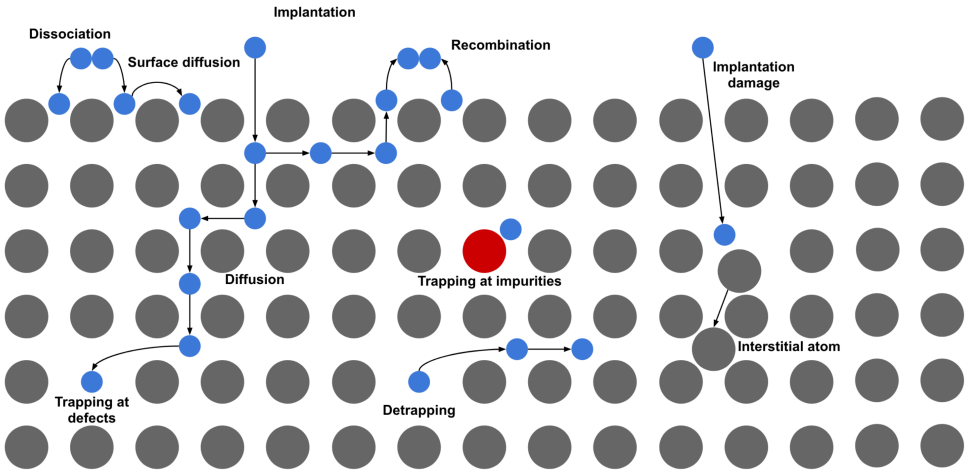

Figure 1.2: Mechanisms of hydrogen diffusion [4].

- $\nabla\cdot$ is the divergence operator
- ∇ is the gradient
- D is the diffusion coefficient

The diffusion coefficient, D, is dependent on temperature and is specific to a material. It can be experimentally determined using techniques such as tracer diffusion experiments or electrochemical methods, or estimated using theoretical models based on molecular dynamics simulations or empirical correlations. D is determined by an equation dependent on the activation energy E_D of a particle diffusing through a material, a pre-exponential factor D_0, and the temperature of the material [9]:

$$D = D_0 \exp(-E_D/k_B T) \tag{1.7}$$

However, there is a clear knowledge gap in our understanding of diffusion coefficients for FLiBe. Fig. 1.3 shows the disparity of diffusion coefficients present in the literature [10]–[15].

However, diffusion through FLiBe is not the only method of hydrogen transport. Hydrogen transport in molten salts involves a combination of mechanisms, including Fickian diffusion and advective transport. Understanding these mechanisms and their governing equations, as well as the calculation of the diffusion coefficient, is essential for predicting and controlling hydrogen transport in molten salt systems.

When a molten salt system is subjected to heat input, such as from nuclear reactions or external heating sources, temperature variations arise, leading to density differences within the fluid. The density differences within the molten salt induce buoyant forces, causing fluid motion through natural convection. Hotter, less dense regions of the molten salt rise while cooler, denser regions descend, establishing convective flow patterns within the system. These flow patterns can transport tritium-containing species along with the bulk fluid motion

The nature of these coupled interactions means that solving for the temperature and fluid flow in a system are inherently linked. A study by Dolan et. al shows that even small temperature gradients of just a few degrees celsius are enough to induce convective

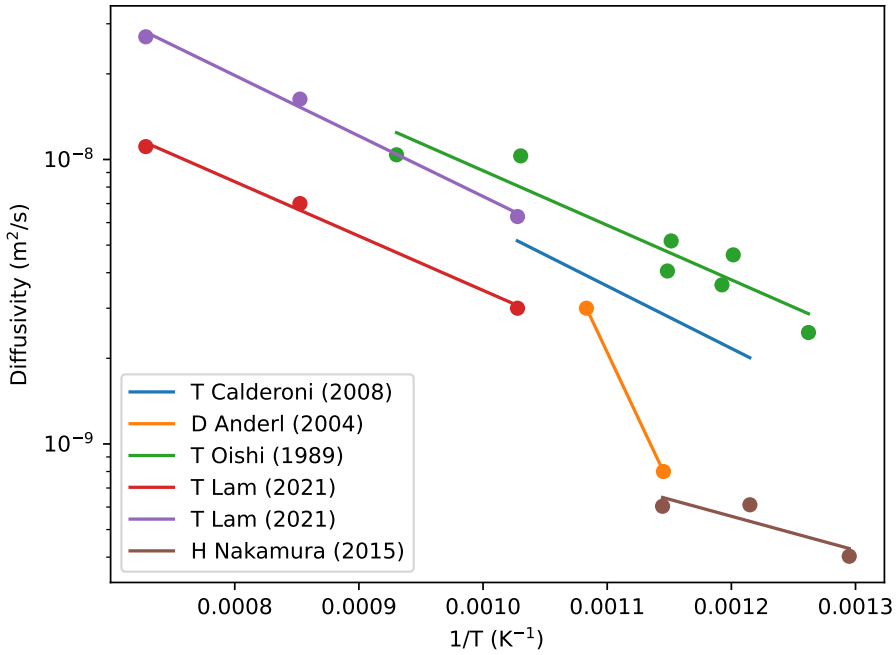

Figure 1.3: FLiBe diffusivity data from literature. Values for diffusivity vary by an order of magnitude at 700 C [16].

flow inside of the molten salt [17]. Considering the massive heat fluxes in a fusion power plant and the high thermal gradients inside of ARC [18], we can expect advective flow to be a heavily contributing transport mechanism for hydrogen inside of a LIB. Understanding the dynamics of diffusive and advective hydrogen transport is crucial for designing safe and efficient molten salt systems for effective LIB design

1.1.5 The LIBRA Experiment

The LIBRA Experiment, a pioneering endeavor in the realm of LIBs, aims to demonstrate the feasibility of efficient Tritium breeding and extraction within a fusion power plant environment [19]. The goals of the LIBRA Experiment include demonstrating tritium self-sufficiency with D-T neutrons, gaining experience with molten salt handling and tritium extraction, and ultimately demonstrating a TBR of about 1. A schematic of the LIBRA Experiment is shown in Fig. 1.4.

BABY, as a scaled-down, 100 mL iteration of LIBRA, offers a unique platform for exploring the intricacies of tritium dynamics and hydrogen transport within the molten salt blanket and serves as a stepping stone to working with molten salts before experimenting with the full 500L LIBRA. A general drawing of BABY is depicted in Fig. 1.5. Two neutron sources provide D-T energy level neutrons from either side and a heater down the center of the cylindrical capsule is constrained to 700 C. A steady flow of helium through the two upper tubes picks up tritium as it dissolves through the top surface of the molten salt where

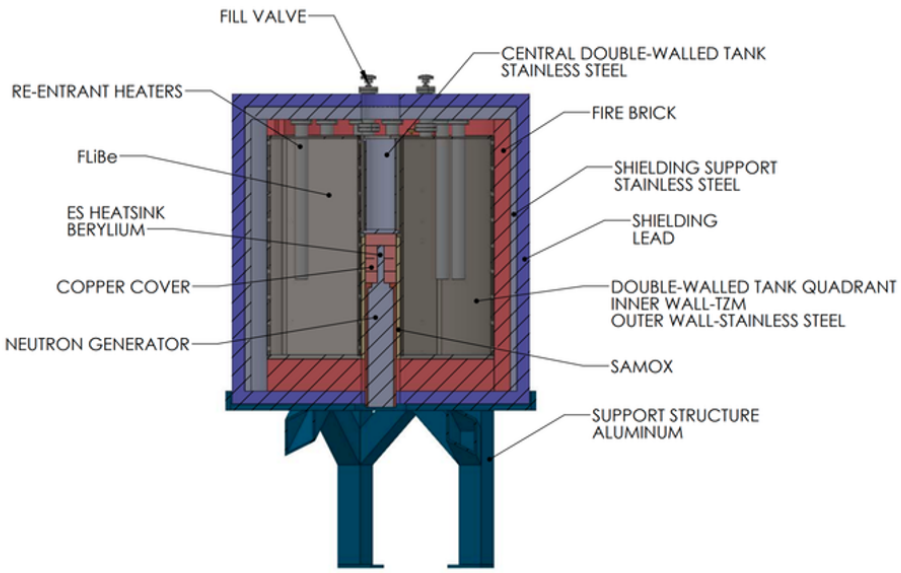

Figure 1.4: LIBRA Experiment Illustration from [19]. Molten FLiBe resides in the capsule with a D-T neutron generator and heater at the center.

it is then collected and counted for TBR calculation.

Experimental results for BABY have already been collected and the LIBRA Experiment team have used a basic zero dimensional model to predict the tritium inventory and release in the salt shown in Fig. 1.6 [20]. While the simple, zero dimensional model can provide valuable insights into tritium transport and release from the salt, it is impossible to know the validity of these results without higher fidelity modeling and experimentation.

Simulating the results for hydrogen transport in BABY is essential for our understanding of tritium transport modeling, and creating models that can effectively predict the tritium retention in fusion power plant systems is essential to creating the first, reliable fusion power plants.

The bulk tritium transport coefficient, k ($\mathrm{m\,s^{-1}}$), is used as a metric for this study. Because the temperature difference from the heater to the outer wall of BABY is unknown, the system is simulated across a range of possible temperature differences. Using the data from a single run, the bulk tritium transport coefficient is calculated in this way:

$$k = \frac{\phi}{A c_{avg}} \tag{1.8}$$

where:

- k is the bulk tritium transport coefficient in $\mathrm{m\,s^{-1}}$
- ϕ is the tritium flux through a surface
- A is the surface area
- c_{avg} is the average concentration of tritium on a surface

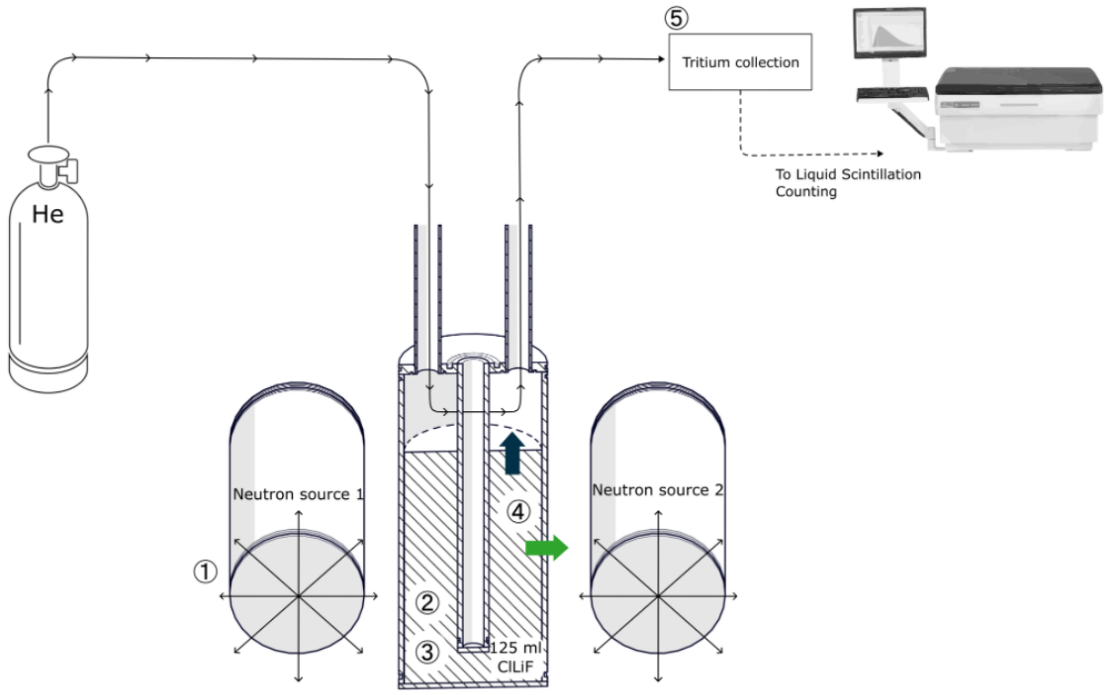

Figure 1.5: Drawing of BABY from [20]. D-T neutron sources (1) irradiate BABY from either side. (2) Tritium producing reactions occur in the salt. (3) Tritium is transported through FLiBe in BABY. (4) Tritium is transported through top surface of FLiBe where it is then collected and counted (5).

This value serves as a metric for assessing the rate of tritium transport out of the salt through the surfaces of FLiBe. For BABY, the bulk tritium transport coefficient for the top surface, which corresponds to the collected tritium was identified as 9.11×10^{-6} m s^{-1}.

Proving that we can create models to accurately simulate tritium transport in molten salt systems is a major stepping stone for LIB and fusion power plant design. In this study, the bulk tritium transport coefficient, as well as the tritium retention and release serve as metrics for assessing the ability to accurately simulate tritium transport in BABY.

While the results from BABY are performed using ClLiF, or Chlorine Lithium Fluoride, simulations are performed using FLiBe for a few reasons. Firstly, lack of data on the thermophysical properties of ClLiF made it a poor choice to simulate with. Next since, FLiBe will eventually be used in a fusion power plant system, it is used for these simulations. While FliBe properties are more documented than ClLiF, their is still a wide spread of properties within the literature that must be taken into account under these simulations.

Having an accurate understanding of how to model tritium transport in BABY and for the LIBRA Experiment is of the utmost importance to tritium transport simulation design, and our ability to model tritium transport phenomena in systems such as LIB's and fusion power plants.

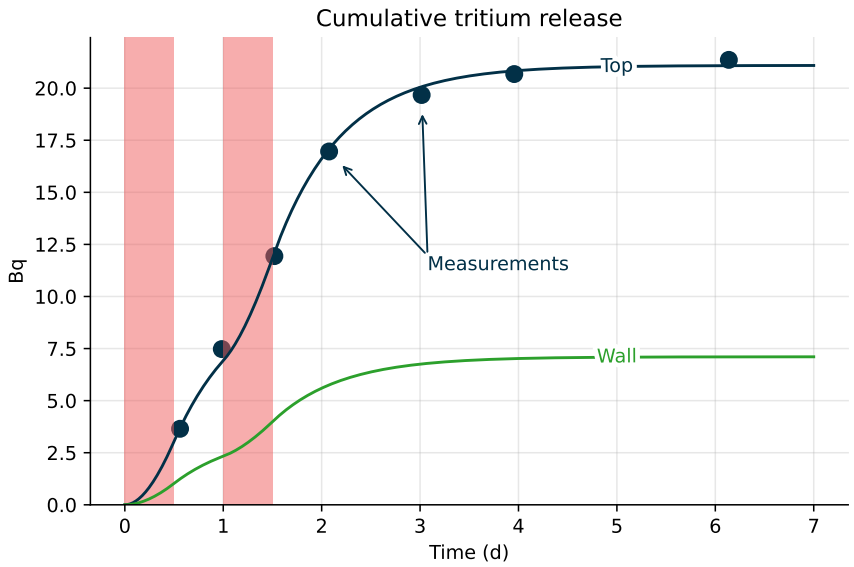

Figure 1.6: Zero dimensional model for hydrogen transport in BABY fit to experimental data. Around 21 Bq tritium is transported through the top surface and nearly 7.5 Bq are transported through the walls.

1.2 Problem Statement

In light of the immense potential of fusion energy to revolutionize global energy production, understanding the underlying physics and engineering challenges associated with fusion power plant designs is paramount. This research contributes to these collective endeavors by elucidating the mechanisms governing hydrogen transport in BABY and simulating tritium transport throughout in steady state and transient conditions. Comparing these simulations to experimental results from BABY will thereby help to advance the frontier of tritium transport simulation and extraction research and pave the way towards practical fusion energy realization.

Chapter 2

Model Description

To comprehensively understand the behavior of hydrogen transport within BABY and its interaction with fluid flow, a multifaceted modeling approach combining computational fluid dynamics (CFD) and diffusion modeling is employed. Integrating fluid flow and heat transfer results of BABY as an input to diffusion simulation proves to be a necessary part of modeling this system due to the complex underlying physics.

The Sherwood number is a dimensionless descriptor of the system that provides insight into the driving mechanisms of mass flow [21]:

$$Sh = \frac{k}{D/L} = \frac{\text{total mass transfer rate}}{\text{diffusion rate}} \tag{2.1}$$

where:

- L is the characteristic length (m)
- D is the mass diffusivity of hydrogen ($\mathrm{m^2\,s^{-1}}$)
- h is the convective mass transfer film coefficient ($\mathrm{m\,s^{-1}}$)

We expect that the Sherwood number is larger than one in the case of this system, meaning that advective flow should have a high effect on the mass transfer rate, and highlighting the importance of this two step simulation process, where the flow of the system is calculated based on an input temperature and then the resulting velocity and temperature fields serve as an input to the diffusion simulation. This section outlines the setup for the simulation model as well as information on mesh generation and the numerical methods used in these simulations.

2.1 Governing Equations

2.1.1 Tritium Transport

The transport of tritium within BABY is governed by the diffusion equation, which describes how the concentration of tritium evolves over time and space due to diffusion, advection, and

any sources or sinks. The diffusion equation for tritium transport can be mathematically expressed as:

$$\frac{\partial c}{\partial t} = \nabla \cdot (D\nabla c) + S - v\nabla c \tag{2.2}$$

where:

- c is the concentration of tritium isotopes
- t is time
- T is the temperature
- D is the temperature dependent diffusion coefficient
- v is the velocity field
- S is the tritium source
- ∇ is the gradient operator,

This equation captures the fundamental mechanisms driving tritium transport within BABY. The first term on the right-hand side represents diffusion, describing how tritium molecules move from regions of higher concentration to regions of lower concentration. The second term accounts for advection, where fluid flow carries tritium along with it, influencing its transport. The third term incorporates any additional sources or sinks of tritium within the system, such as tritium production or extraction processes.

The velocity field and temperature field inputs have significant input on tritium transport. A constant source of 1.83×10^5 $\mathrm{T\,s^{-1}}$ tritium is applied to the volume. This is a measured quantity calculated from real experimental data based on the number of neutrons provided by the neutron generator. The temperature field also directly impacts the value of the diffusion coefficient.

By solving the diffusion equation with inputs being the corresponding temperature and velocity fields, we can model the transport of tritium within BABY and gain insights into its behavior under different operating conditions.

2.1.2 Heat Transport

The temperature field within BABY is governed by the heat transfer equation, which describes how thermal energy is transferred and distributed within the system. This equation considers the mechanisms of conduction and advection to accurately model the temperature distribution across BABY. The governing equation for solving the temperature field in BABY can be expressed as follows:

$$\frac{\partial \mathbf{T}}{\partial t} = \nabla \cdot \left(\frac{\lambda}{\rho c_p} \nabla \mathbf{T} \right) - \mathbf{v}\nabla \mathbf{T} \tag{2.3}$$

where:

- ρ is the fluid density,
- c_p is the specific heat capacity at constant pressure,
- T is the temperature,
- t is time,
- $\mathbf{v}$ is the velocity vector field,
- λ is the thermal conductivity,
- ∇ is the nabla operator (gradient),

This equation accounts for the diffusion of thermal energy through BABY due to temperature gradients as well as the transfer of heat through the velocity field and is solved in conjunction with the Navier-Stokes equations for fluid flow. Accurately predicting the temperature distribution within BABY enables us to analyze the effects of temperature variations within BABY on diffusive mechanisms such as the diffusion coefficient and fluid flow.

2.1.3 Navier Stokes

The velocity field within BABY is determined by the Navier-Stokes equations, which describe the motion of fluid flow within the reactor components. In conjunction with the Boussinesq approximation, these equations account for the effects of buoyancy-driven flow due to temperature variations, providing a comprehensive framework for modeling convective heat transfer and fluid dynamics in the system. The Navier-Stokes equations for incompressible flow with the Boussinesq approximation govern the momentum conservation of fluid particles and are given by:

$$\frac{\partial v}{\partial t} + (v \cdot \nabla)v = -\frac{1}{\rho}\nabla p + \nu\nabla^2 v - g\alpha\,(T - T_0) \tag{2.4}$$

$$\nabla \cdot v = 0 \tag{2.5}$$

where:

- ρ is the fluid density
- v is the velocity vector field
- t is time
- p is the pressure
- ν is the kinematic viscosity
- ∇ is the nabla operator (gradient)

- ∇^2 is the Laplacian operator (divergence of gradient)
- g is gravitational acceleration
- α is thermal expansion coefficient
- T is the temperature vector field
- T_0 is the bulk temperature of the fluid
- Equation (2.4) is the momentum equation.
- Equation (2.5) is the continuity equation.

The Boussinesq approximation is a simplification for natural convection and other buoyancy-driven flow that assumes the density of the fluid remains approximately constant, except in the buoyancy term of the momentum equation [22]. These equations represent fluid flow in BABY, accounting for convective acceleration, pressure gradients, viscous forces, and gravitational forces. They provide a mathematical framework for solving for the velocity field within BABY under the influence of external forces and boundary conditions.

By solving the Navier-Stokes equations with the Boussinesq approximation and appropriate boundary and initial conditions, we can accurately predict the velocity velocity field in tandem with the temperature field to determine how these inputs impact tritium transport throughout BABY.

2.2 Numerical Methods

2.2.1 Finite Element and FEniCS

The Finite Element Method (FEM) is a numerical technique used for solving partial differential equations (PDEs) and modeling physical phenomena in various engineering and scientific applications. FEM discretizes the domain of interest into smaller, simpler elements, allowing for the approximation of the solution to the governing equations within each element. These discrete approximations are then assembled into a global system of equations, which can be solved to obtain the solution over the entire domain [23].

Some key concepts of finite element modeling are very important. Discretizing the domain of interest into smaller geometric entities called elements. Each element is described by a set of nodes, and the solution within each element is approximated using interpolation functions, typically polynomial in nature. The discrete equations within each element are assembled into a global system of equations, accounting for the coupling between neighboring elements through shared nodes or boundaries. The global system of equations is then solved using iterative solvers in this case. The solution provides the approximate values of the unknowns throughout the domain.

FEniCS, a popular open-source finite element (FE) library that allows for solving the CFD PDEs numerically, was utilized for solving the PDEs governing fluid flow and heat transfer within BABY [24]. FEniCS was chosen in place of other PDE solvers for its integration with

the diffusion solver used in this project and coding interface that allows for easy parametric modeling for batch simulations with differing input conditions. By reading the mesh data from the XDMF file format, FEniCS enables accurate and efficient numerical simulations, providing insights into fluid dynamics and hydrogen transport phenomena.

2.2.2 FESTIM

FESTIM is a computational tool specifically designed for modeling the transport of tritium and other hydrogen isotopes in systems. FESTIM utilizes finite element methods to solve the diffusion equations governing hydrogen transport, accounting for various transport mechanisms such as diffusion and advection [25]. FESTIM leverages the capabilities of FEniCS to solve the PDE's relating to tritium transport.

The temperature and velocity fields served as essential inputs to the tritium transport simulation within FESTIM. In FESTIM, the temperature and velocity fields obtained from the CFD simulations were utilized to drive the tritium transport simulation. The governing equations for tritium diffusion, incorporating the effects of temperature gradients and fluid flow, were solved numerically using finite element methods within the FEniCS framework.

2.2.3 Meshing

The meshing process is a critical step in finite element modeling, determining the accuracy and efficiency of the numerical solution. In this study, the mesh for the BABY system was generated using the SALOME platform [26], a powerful tool for pre-processing. To exploit the axial symmetry of the system and reduce computational cost, a cross-section of the cylindrical mesh was taken. Specifically, the right half of the symmetric sides was selected for mesh generation. This approach effectively reduces the computational domain while preserving the essential features of the system. Fig. 2.1 shows a representation of the cylindrical cross section taken from BABY along with the corresponding mesh generated in SALOME as well as names for the corresponding edges of the mesh that will be referred to in the rest of this paper.

The mesh was generated in SALOME with a total count of 42,478 nodes. A gradient in node density was applied around the edges of the surface to better model the complex interactions around mesh edges in the flow. It was then exported to the XDMF format and used for solving the finite element model.

2.2.4 Boundary Conditions

The accurate specification of boundary conditions (BCs) is essential for realistic and reliable numerical simulations. In this section, we outline the boundary conditions utilized in finite element modeling of BABY. Because there are three sets of equations relating tritium transport, heat transport, and Navier Stokes three sets of boundary conditions are needed to constrain the model. Fig. 2.2 shows a representation of the flow, temperature, and tritium transport boundary conditions imposed on the model.

At the top surface of the system, a slip boundary condition is applied. This condition allows fluid particles to slide freely along the surface without sticking, simulating a lack of

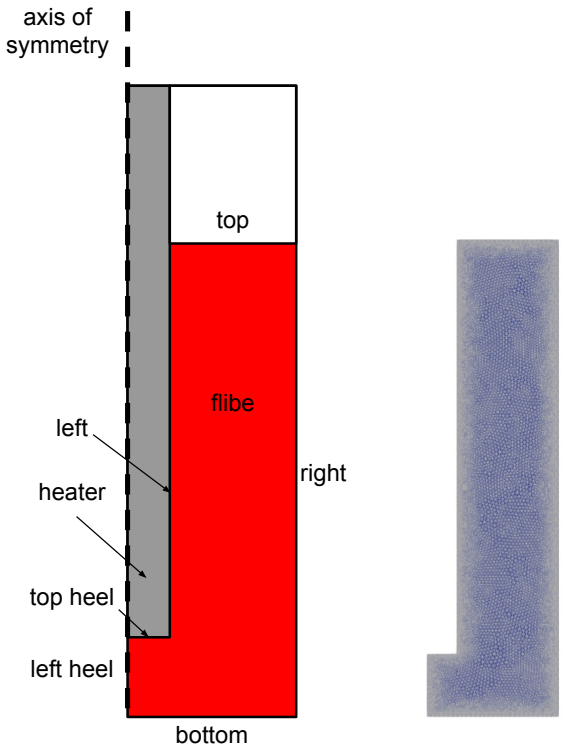

Figure 2.1: Cross section of BABY with labels for relevant surfaces including top, bottom, right, left, left heel, and top heel with SALOME mesh on right. SALOME mesh has a total node count of 42,478 with an increased density around the edges for finer boundary layer modeling.

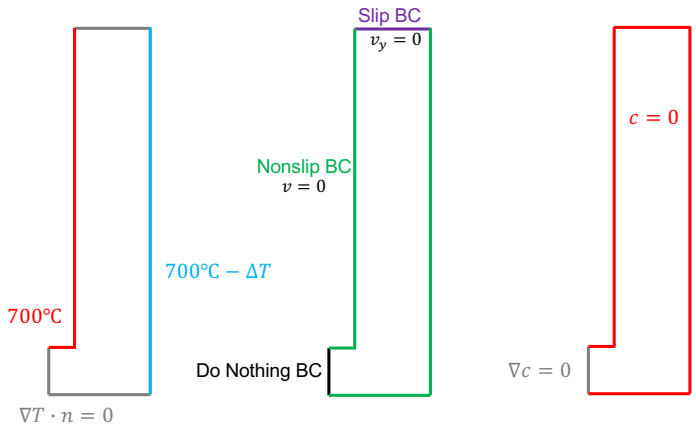

Figure 2.2: Boundary conditions for tritium transport, heat transport, and tritium transport in BABY

fluid-solid interaction which is representative of he low friction of air flowing over the top. Along the top heel, left, bottom, and right sides of the reactor system, no-slip boundary conditions are enforced. These conditions dictate that the fluid velocity is zero at the walls, mimicking the adhesion of the fluid to the solid boundaries. On the left heel of the reactor system, which lies on the axis of symmetry, a "do nothing" boundary condition is applied. This condition imposes no constraints on the flow, allowing it to evolve naturally without any specified velocity or pressure boundary conditions.

For the heat transfer boundary conditions, the left and top heel surfaces of the mesh, representing the regions in direct contact with the heater, are constrained to maintain a temperature of 700 degrees Celsius, which is a measured temperature of the system. The right surface is constrained to maintain a temperature of 700 degrees Celsius minus an input temperature difference. Since the actual temperature of the outer wall is unknown, the results are simulated across a range of possible temperature differences to encapsulate the possible flow conditions. The remaining surfaces of the reactor system are constrained to have no temperature flux through the surface. This condition ensures that there is no heat transfer across these surfaces, effectively insulating them from external temperature variations and maintaining adiabatic conditions.

By imposing these boundary conditions, we effectively control the thermal and flow behaviors of the BABY system, guiding the temperature distribution and heat transfer processes within the fluid. These boundary conditions play a crucial role in simulating realistic operating conditions.

For the tritium transport boundary conditions, at the left heel surface of the reactor system, which lies on the axis of symmetry, a gradient boundary condition is specified to maintain continuity in concentration gradients. Specifically, the gradient of the concentration $\nabla c = 0$. This condition ensures that there is no flux of particles across the left heel boundary, maintaining a continuous concentration profile along the axis of symmetry.

For all other surfaces including the top, right, bottom, left, and top heel surfaces, a Dirichlet boundary condition is applied. In this case, the concentration of hydrogen isotopes $c = 0$. This boundary condition implies that there is no accumulation of particles at these

surfaces, allowing diffusing particles to freely exit the computational domain.

2.3 Model Description Summary

The methods described in these sections lay the framework for results that accurately predict tritium transport in the BABY system. By elucidating simulation setup including meshing, equations that are being solved, and boundary conditions used in simulation, the results for tritium transport of BABY can be predictably described to within a finite range for steady state and transient simulations of the system.

Chapter 3

Results

3.1 Fluid Flow and Heat Transfer

Results for fluid flow and temperature distributions in BABY were simulated for varying temperature differences from the heater to the outer wall ranging from 0 to 10 °C. Varying this input showed that increasing the temperature difference across BABY caused for faster advective flow within the system and lager thermal gradients, which is an expected result for the system. Results for a range of temperature differences and thermal gradients are pictured in 3.1.

All results for these studies are simulated to steady state which involves reaching a condition where the system's behavior no longer changes with time, indicating a balance between all relevant processes. Since BABY is held under heating conditions for twelve hours before beginning its irradiation schedule, the fluid flow within BABY is assumed to already be at steady state before experimenting on the system. This is reflected in the model by allowing all fluid flow and heat transfer simulations to run to steady state.

In the context of this model and its governing equations, simulating to steady state means that $\frac{\partial v}{\partial t} = 0$ and $\frac{\partial T}{\partial t} = 0$ for the heat transfer and Navier-Stokes equations described previously.

To ensure the accuracy and reliability of these results, fluid flow and heat transfer simulation results were compared against a simulation using COMSOL Multiphysics software under the same input conditions with a temperature difference of 2 °C across the salt. Fig. 3.2 presents the findings of the comparison between the two simulation platforms.

The comparison between the CFD results obtained from the simulations in FEniCS and COMSOL Multiphysics demonstrated good agreement in fluid flow patterns and temperature distributions within BABY. The consistency between the two simulation platforms validates the accuracy of the CFD results and reinforces confidence in the predictive capabilities of the computational models. This verification process enhances the reliability of the simulation findings and provides valuable insights into the fluid dynamics and thermal behavior of the system.

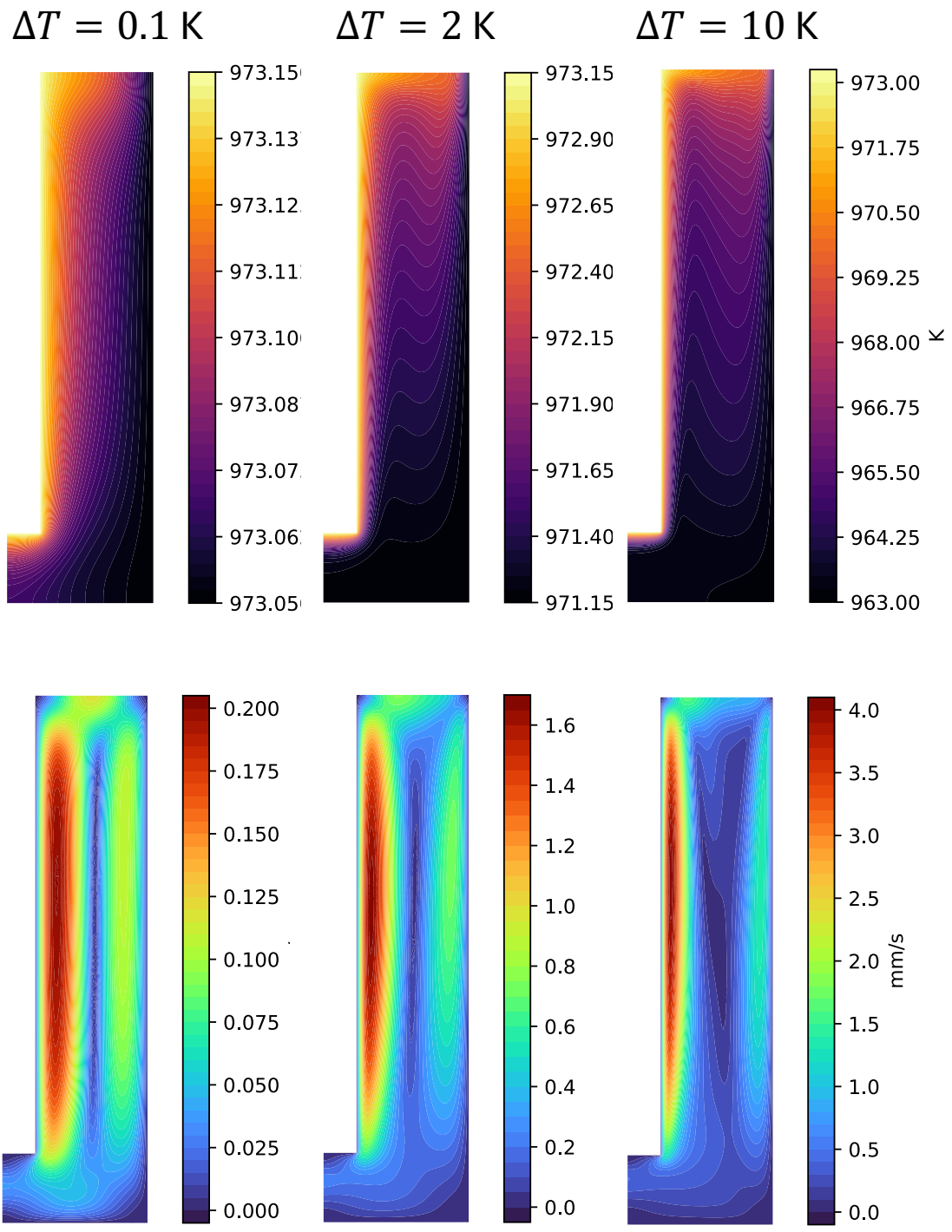

Figure 3.1: Results for steady state simulations of BABY at temperature differences of 0.1, 2, and 10 25 °C. Increasing temperature difference shows increase in advective flow and stronger thermal gradients in FLiBe.

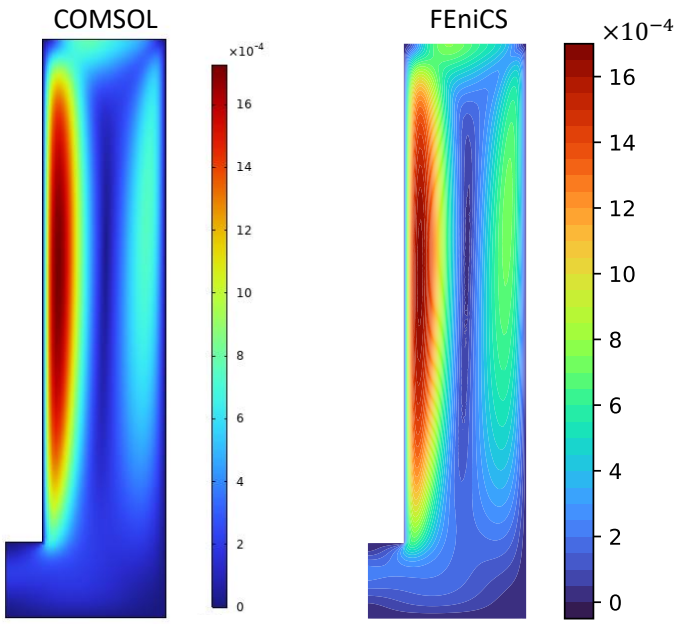

Figure 3.2: FEniCS fluid flow simulation validation with COMSOL shows good agreement between created FEniCS model and COMSOL Multiphysics simulation

3.2 Tritium Transport

Steady-state simulations of BABY were conducted to investigate the influence of temperature differences on tritium transport. The simulations varied the temperature difference across BABY within the range of 0 to 10 °C, while assessing the impact on tritium transport through FLiBe. This range encompasses realistic operational conditions and allows for a comprehensive analysis of temperature-dependent tritium transport. Details about important system parameters including volume, surface areas, the tritium source, and bounds for diffusivities used in the simulation are shown in Table 3.1:

Table 3.1: System parameters for BABY simulation including volume, area of top surface and walls, tritium source, and diffusion simulation bounds

Parameter	**Value**
V	5.804×10^{-5} m^3
A_{top}	7.53×10^{-4} m^2
A_{walls}	1.345×10^{-2} m^2
S	1.83×10^{5} T/s
D	$[3.17 \times 10^{1} \cdot \exp(-1.84/k_{\text{B}}T),\ 1.51 \times 10^{-8} \cdot \exp(-0.24/k_{\text{B}}T)]$

Results from fluid flow and heat transfer simulations had direct impacts on tritium transport. Fig. 3.3 shows the influence of the temperature difference on the concentration of tritium in the salt at steady state for a range of temperature differences. Larger temperature differences caused for higher transport of tritium around the edges of the model that resulted

in lower concentrations in those areas, however, slightly higher concentrations were simulated near the center of the circular motion of fluid for the higher temperature differences.

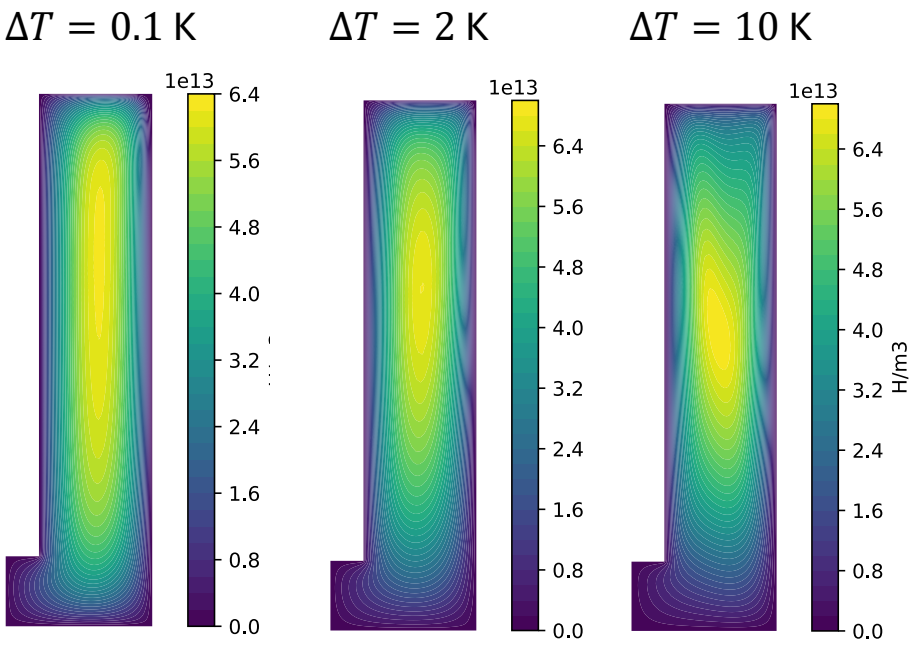

Figure 3.3: Steady state simulations of concentration for temperature differences of 0.1, 2, and 10 °C. High temperature differences show large changes in tritium concentration throughout FLiBe.

The bulk tritium transport coefficient from Eq. 1.8 is used as a metric for this study. Because the temperature difference from the heater to the outer wall of BABY is unknown, the curve relating temperature difference to the tritium transport coefficient provides insights about tritium extraction and accurately computing its factors is very important. The average concentration of tritium at a surface was computed using:

$$c_{\text{avg}} = \frac{\int c \cdot r dr}{\int r dr} \tag{3.1}$$

where:

- c_{avg} is the average concentration of tritium on the surface
- r is the radial distance
- dr is the differential element of the radial distance
- $\int$ is the integral operator

The tritium flux through the surface was calculated using:

$$\phi = \int -D\nabla c \cdot n dS \tag{3.2}$$

where:

- ϕ is the tritium flux through the surface
- $\int$ is the integral operator
- D is the diffusion coefficient
- ∇ is the gradient operator
- c is the concentration
- n is the surface normal vector
- dS is the differential element of the surface

Calculating these values for the bulk tritium transport coefficient represents the rate of tritium extraction in FLiBe under different temperature conditions. Their dependencies are graphed in Fig. 3.4.

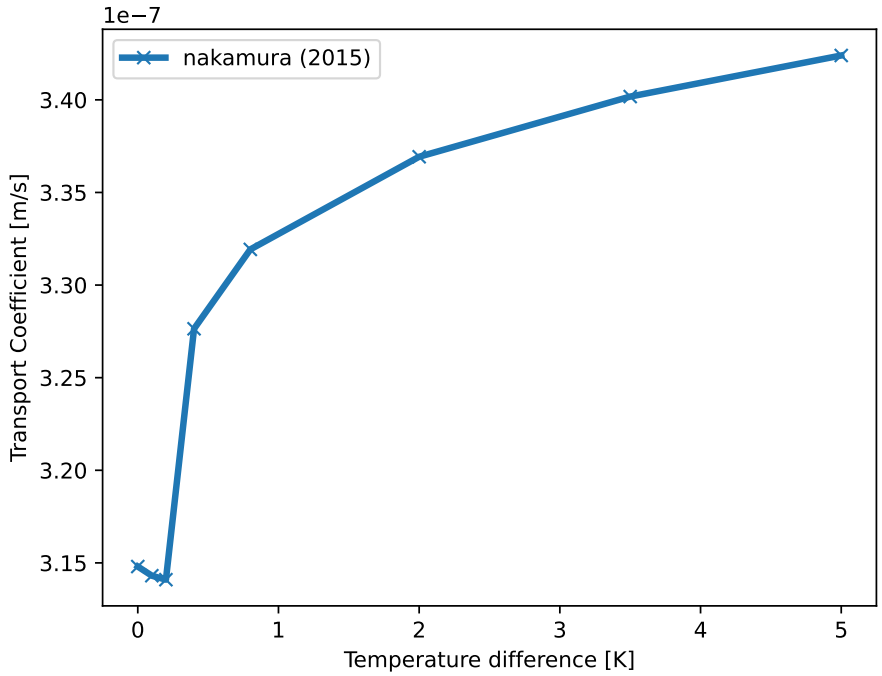

Figure 3.4: Steady state simulation of BABY using Nakamura's value for diffusivity. Shows large increase in tritium transport coefficients for small temperature differences before gradual leveling out.

The results of the steady-state simulations revealed a notable dependence of tritium transport coefficients on the temperature difference across BABY for temperature differences above 0.25 °C. This is presumably due to the induction of naturally convective flow in the FLiBe at the advent of the temperature difference.

To assess the validity of these results in context of the vast array of data on the physical, thermal, and chemical properties of FLiBe present in the literature, a few properties are analyzed that would have the largest effect on tritium transport.

Curves relating data for the bulk tritium transport coefficient to the temperature difference across BABY for viscosity [27]–[30], density[31]–[36] and diffusion are shown in Fig. 3.5.

While it was originally expected that thermophysical properties like density and viscosity would have a large effect on the results obtained from the simulation considering the speed of advective flow in relation to diffusive tritium transport, and the use of the Boussinesq approximation which relies heavily on density to determine buoyancy forces, these properties had little effect on the bulk tritium transport coefficient.

On the other hand, diffusivity had a massive impact on the bulk tritium transport coefficient, with results varying nearly an order of magnitude. For this reason, results for steady state and transient simulations are presented as a range of possible values, with the upper bound being simulated using Anderl's value for diffusivity, and the lower bound being simulated using Nakamura's value for diffusivity in Fig. 3.6.

When comparing these results that take into account the uncertainty in simulation results due to variance in FLiBe diffusivity, we see that the measured value for the tritium transport coefficient in BABY fits neatly in between these two curves. This suggests that these bounds, though large, provide a reasonable range for simulating the tritium transport coefficient in BABY

3.3 Transient Results

While the fluid flow and heat transfer inside of BABY are assumed to be at steady state, we know that during irradiation of BABY, the tritium transport is not at steady state. Transient simulations of BABY were conducted to investigate the time-dependent behavior of tritium transport under irradiation conditions. These simulations were performed at a temperature difference of 2 °C. across BABY to assess the dynamics of tritium flux and release through the various surfaces. These surface release profiles were analyzed over time to understand the transient response of the system.

The same tritium source of 1.83×10^5 $\mathrm{T\,s^{-1}}$ was applied, however, its application was applied piece-wise over a seven day period for the first and third twelve hour periods. The fluid flow and heat transfer simulations are again simulated to steady state, but the steady state velocity and temperature fields are used to inform the transient tritium transport simulation starting from zero seconds. This scheme accurately reflects the experimental procedure employed by the LIBRA group and the results from these simulations are presented in Fig. 3.7.

Results for cumulative tritium release are calculated in Becquerel (Bq) which is a measure of the radioactivity of a substance using:

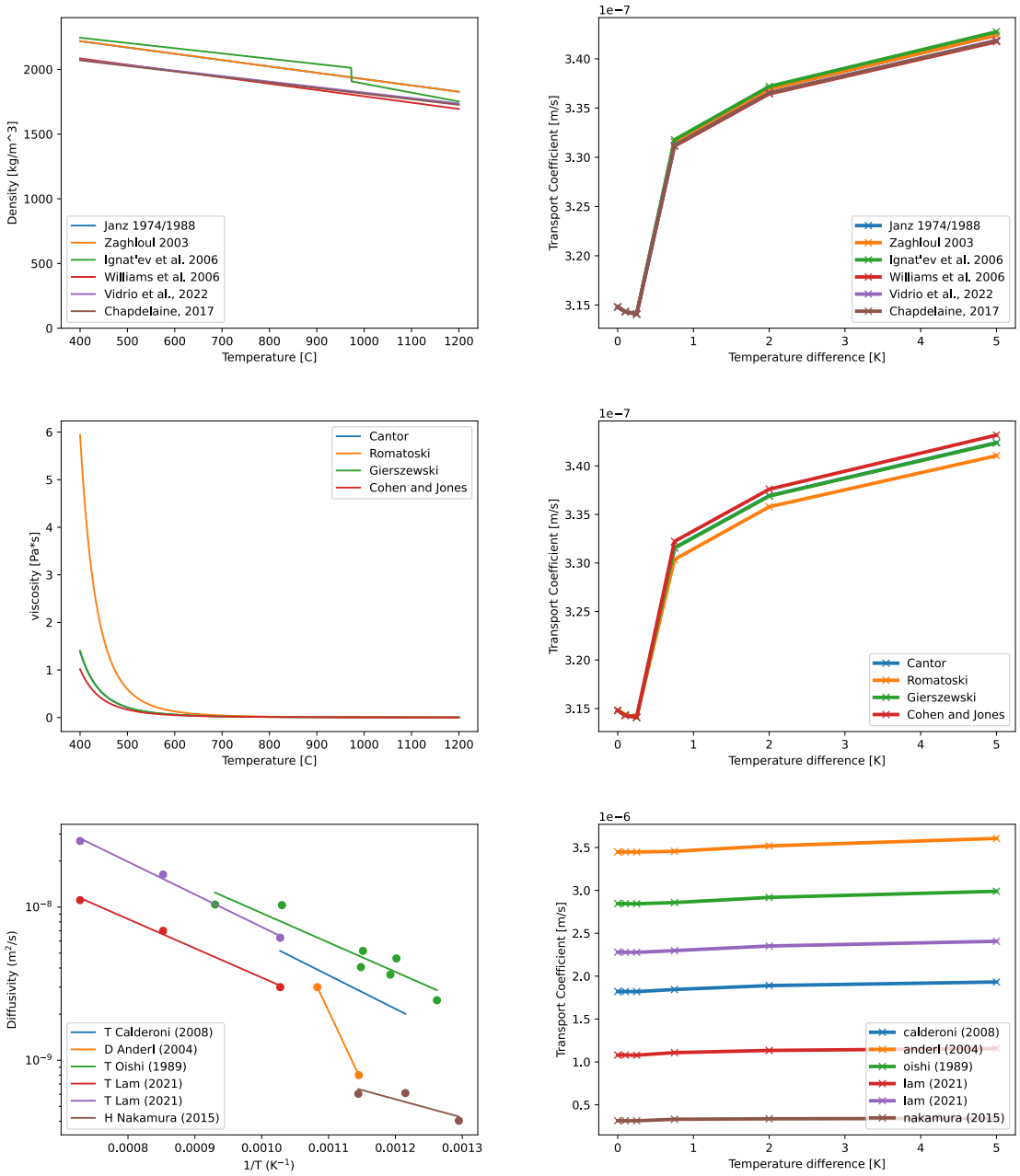

Figure 3.5: Property study on the impact of relevant FLiBe physical properties on tritium transport coefficient. thermophysical properties showed low sensitivity to variation, however diffusivity varied on the order of a magnitude.

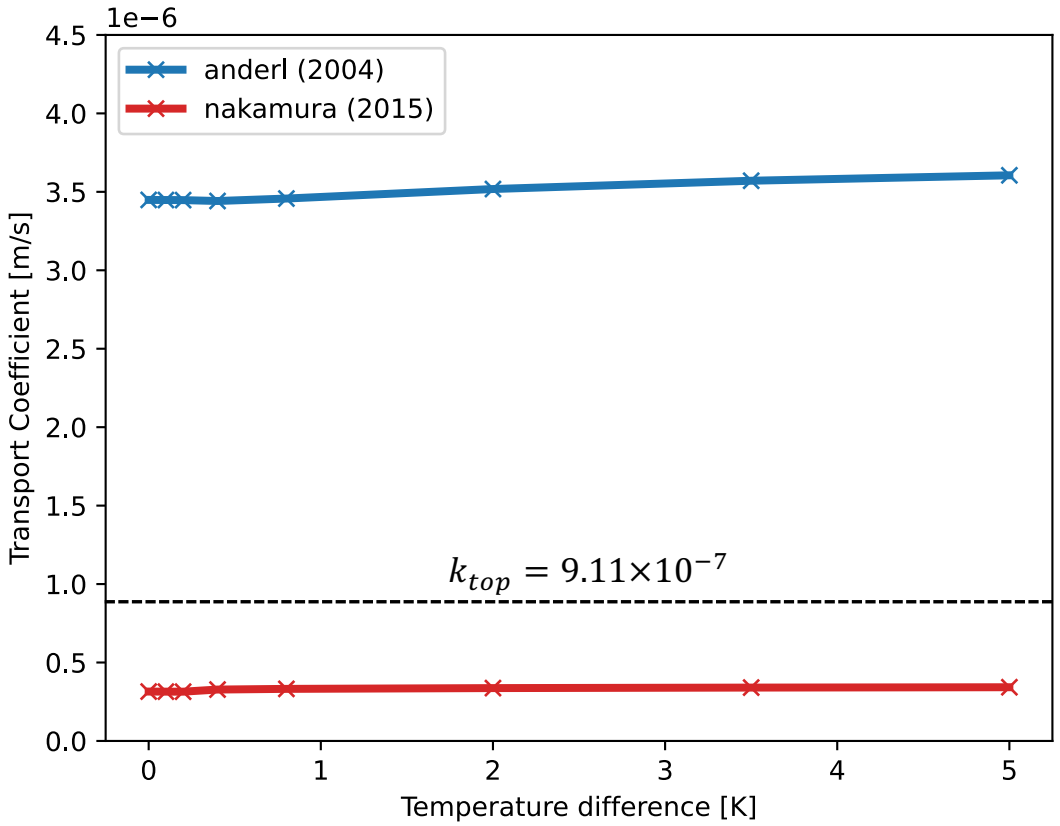

Figure 3.6: Steady state tritium transport coefficients for upper and lower bounds of diffusivities given by Nakamura and Anderl. The measured tritium transport coefficient of 9.11×10^{-7} m s^{-1} fits in between the two curves.

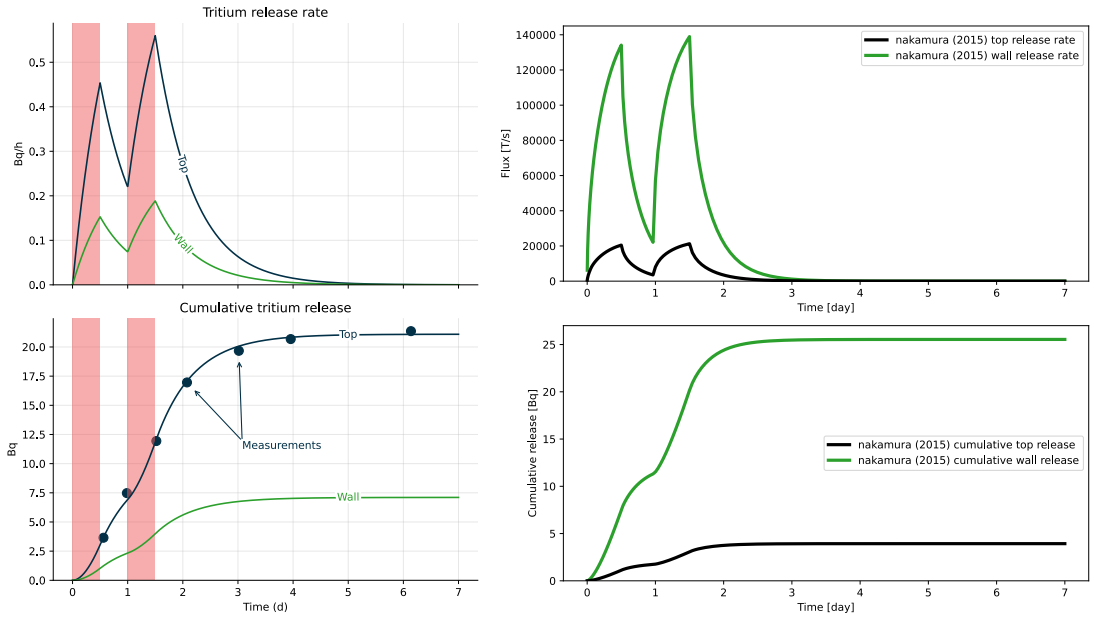

Figure 3.7: Simulated transient tritium flux and release using Nakamura's diffusivity on the right vs measured tritium transport and release from BABY Experiment on the left. Shaded red areas represent 12 hour irradiation schedules.

$$Q_{Bq} = \frac{Q_T M_T A_T}{N_A} \tag{3.3}$$

where:

- Q_{Bq} is the quantity of tritium in Becquerel
- Q_{T} is the quantity of tritium
- M_{T} is the molar mass of tritium
- A_{T} is the specific activity of tritium
- N_{A} is Avogadro's Number

The transient simulations revealed dynamic fluctuations in surface flux and release profiles as the system responded to irradiation and thermal gradients. Initially, a rapid increase in surface flux and release was observed, reflecting the onset of tritium production and diffusion within BABY. It took approximately 3 days from the beginning of the day and a half irradiation schedule for the system to reach a steady-state condition, where the surface flux and release profiles stabilized. This period of transient behavior highlights the time required for tritium transport processes to equilibrate and for the system to achieve a balanced state post irradiation conditions.

This behavior closely mimics experimental data for the irradiation schedule of BABY apart from one major difference. Notably, the flux through the top surface of BABY was

observed to be significantly smaller than that through the walls. This observation directly conflicts with experimental measurements. A total of 29.47 Bq were distributed into the salt, of which 3.93 Bq diffused through the top, 25.54 Bq diffused through the walls, and a small portion of 2.32×10^{-6} Bq remained in the FLiBe at the end of the seven day simulation.

The simulation was then studied under the same uncertainty bounds described by Nakamura's and Anderl's diffusivities in the previous section. Fig. 3.8 depicts the results for the varying diffusivities on cumulative releases and surface fluxes.

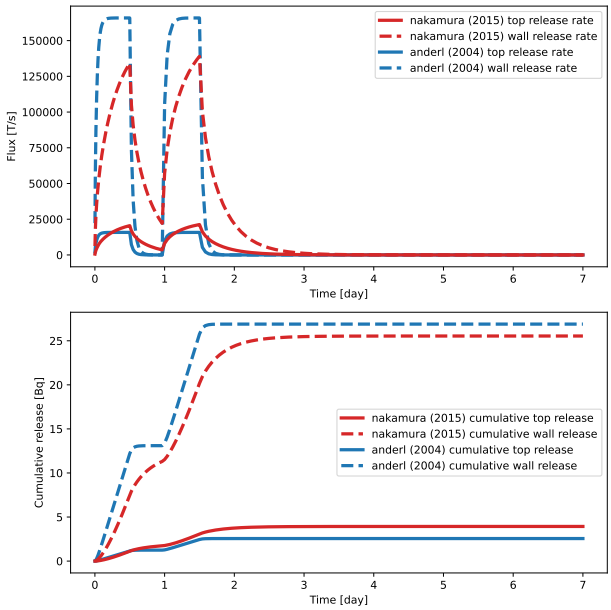

Figure 3.8: Transient

Higher diffusivity exhibited a much faster transient response to irradiation. The distribution of tritium released through the top and sides of the model changed slightly due to the change in diffusivities as well. Where the top release was 3.93 Bq and the walls were 25.54 Bq for the lower diffusivity, the top release decreased to 2.56 Bq and the wall release increased to 26.89 Bq for the higher diffusivity.

The results of transient simulations provide valuable insights into the time-dependent behavior of tritium transport in the BABY system under irradiation conditions. By examining the transient response of wall flux and release profiles, this analysis enhances our understanding of tritium management strategies and informs the design and operation of fusion power plant systems utilizing molten salt blankets.

Chapter 4

Conclusion

4.1 Discussion

In this study, comprehensive simulations to investigate tritium transport phenomena within BABY have been conducted with a focus on both steady-state and transient conditions. By integrating fluid flow and heat transfer simulations with diffusion modeling using FESTIM, valuable insights into the complex interplay between fluid flow, temperature gradients, and tritium migration in molten salt blankets have been gained.

Steady state simulations revealed the large dependency of tritium transport coefficients on the diffusivity of FLiBe, which accounts for a wide range of possible results considering the knowledge gap in literature, and a wide range of properties that have been identified for FLiBe. By systematically varying the temperature difference and calculating tritium transport coefficients for upper and lower bounds of FLiBe diffusivities, the range of possible tritium transport coefficients for the system under steady state conditions for a range of temperature differences have been identified to well encompass the experimentally determined BABY tritium transport coefficient.

While steady state simulations showed good agreement between experimentally determined values for bulk tritium transport, transient simulations provided some expected and unexpected insights into the complex behaviors of tritium transport in molten salt systems. By mimicking the irradiation schedule of BABY, the time dependent behavior of tritium transport under irradiation conditions have been elucidated.

At the ranges of diffusivities for FLiBe, a steady state settling time ranged from one to two days to just hours depending on the diffusivity used from the literature. The chosen diffusivity of FLiBe also had implications on the raito of tritium transported through the top surface to that transported through the walls, with the upper diffusivity bound having less tritium transported through the top.

A notable discrepancy between the experimental tritium release and the simulated release from this paper was the inverse relation that tritium transport had through the top surface and through the walls. This difference hints at the complex mechanisms driving tritium transport in molten salt systems and suggests that more complex modeling may be needed for transient simulations of tritium transport that account for other possible contributing factors such as salt chemistry and speciation of tritium in the salt.

The insights gained from this study have important implications for the design and operation of fusion power plant systems utilizing molten salt blankets. By considering the complex interactions between fluid flow, temperature gradients, and tritium transport, we can develop effective tritium management strategies to enhance power plant performance, safety, and sustainability. The integration of fluid flow and heat transfer with diffusion modeling techniques provides a powerful framework for investigating tritium transport phenomena and guiding the development of advanced fusion power plant concepts.

4.2 Future Work

The natural continuation of this work is to expand the analysis of this study onto the next systems of the LIBRA Experiment including the 1 liter and full LIBRA iterations. The framework for CFD and diffusion analysis has already been laid down for a streamlined approach to simulating tritium transport phenomena within these systems as well as more complex systems including fusion power plants or fission plants utilizing molten salt technologies. Further research into this area will help to validate the results obtained through these methods and to further our understanding of the complex interactions of tritium in an LIB setting.

A major area of uncertainty in the literature that has been identified through this work is research into the thermophysical and diffusive properties of molten salts. If molten salt systems are going to be reliably simulated and implemented into fusion power plant or LIB designs, our understanding of the fundamental constants driving these processes will have to be investigated and reliably determined. Further research to determine constants such as diffusivity and density of FliBe will increase the credibility and reliability of this research.

Lastly, the processes driving tritium diffusion have been heavily simplified to efficiently model the tritium transport of this system. Future work will seek to incorporate the physical and chemical interactions driving tritium transport in an LIB system such as multi-species simulation of hydrogen and assessment of the chemical reactions also impacting tritium flow to better encapsulate all of the forces at play for this complex system.

Overall, this research lays down the foundation for in depth simulation and analysis of future iterations of BABY with room to expand to more complex systems such as fusion power plant and LIB design. The results of this study will be used to guide research into tritium transport modeling as it relates to the LIBRA Experiment, and the greater area LIB and fusion power plant design.

References

[1] A. Köhn-Seemann and J. Hillairet, *Alfkoehn/fusion_plots: Second release of the fusion plot package (new plots added)*, Jun. 2021. DOI: 10.5281/zenodo.4946068. URL: https://doi.org/10.5281/zenodo.4946068.

[2] I. A. E. Agency, *Development of a methodology for measuring deuterium-tritium fuel in dt fusion experiments by neutron detection*, https://inis.iaea.org/search/search.aspx?orig_q=RN:44045168, 2022.

[3] M. Kovari, M. Coleman, I. Cristescu, and R. Smith, "Tritium resources available for fusion reactors," en, *Nuclear Fusion*, vol. 58, no. 2, p. 026 010, Feb. 2018, ISSN: 0029-5515, 1741-4326. DOI: 10.1088/1741-4326/aa9d25. URL: https://iopscience.iop.org/article/10.1088/1741-4326/aa9d25 (visited on 04/24/2024).

[4] R. Delaporte-Mathurin, "Hydrogen transport in tokamaks," en,

[5] M. Nagumo, *Fundamentals of Hydrogen Embrittlement*, en. Singapore: Springer Singapore, 2016, ISBN: 978-981-10-0160-4 978-981-10-0161-1. DOI: 10.1007/978-981-10-0161-1. URL: http://link.springer.com/10.1007/978-981-10-0161-1 (visited on 04/24/2024).

[6] K. C. Jordan, B. C. Blane, and W. A. Dudley, "HALF-LIFE OF TRITIUM," en,

[7] M. Abdou, M. Riva, A. Ying, C. Day, A. Loarte, L. Baylor, P. Humrickhouse, T. F. Fuerst, and S. Cho, "Physics and technology considerations for the deuterium–tritium fuel cycle and conditions for tritium fuel self sufficiency," en, *Nuclear Fusion*, vol. 61, no. 1, p. 013 001, Jan. 2021, ISSN: 0029-5515, 1741-4326. DOI: 10.1088/1741-4326/abbf35. URL: https://iopscience.iop.org/article/10.1088/1741-4326/abbf35 (visited on 04/24/2024).

[8] B. Sorbom, J. Ball, T. Palmer, *et al.*, "ARC: A compact, high-field, fusion nuclear science facility and demonstration power plant with demountable magnets," en, *Fusion Engineering and Design*, vol. 100, pp. 378–405, Nov. 2015, ISSN: 09203796. DOI: 10.1016/j.fusengdes.2015.07.008. URL: https://linkinghub.elsevier.com/retrieve/pii/S0920379615302337 (visited on 03/13/2023).

[9] E. L. Cussler, *Diffusion: mass transfer in fluid systems*, en, 3. ed., 4. printing. Cambridge: Cambridge Univ. Press, 2011, ISBN: 978-0-521-87121-1.

[10] P. Calderoni, P. Sharpe, M. Hara, and Y. Oya, "Measurement of tritium permeation in flibe (2LiF–BeF2)," *Fusion Engineering and Design*, vol. 83, no. 7, pp. 1331–1334, 2008, ISSN: 0920-3796. DOI: https://doi.org/10.1016/j.fusengdes.2008.05.016. URL: https://www.sciencedirect.com/science/article/pii/S0920379608000926.

[11] R. Anderl, S. Fukada, G. Smolik, *et al.*, "Deuterium/tritium behavior in Flibe and Flibe-facing materials," *Proceedings of the 11th International Conference on Fusion Reactor Materials (ICFRM-11)*, vol. 329-333, pp. 1327–1331, Aug. 2004, ISSN: 0022-3115. DOI: 10.1016/j.jnucmat.2004.04.220. URL: https://www.sciencedirect.com/science/article/pii/S0022311504003952.

[12] J. Oishi, H. Moriyama, S. Maeda, and Y. Asaoka, "Tritium recovery from molten LiF-BeF2 salt," *Fusion Engineering and Design*, vol. 8, pp. 317–321, 1989, ISSN: 0920-3796. DOI: https://doi.org/10.1016/S0920-3796(89)80124-3. URL: https://www.sciencedirect.com/science/article/pii/S0920379689801243.

[13] S. T. Lam, Q.-J. Li, R. Ballinger, C. Forsberg, and J. Li, "Modeling LiF and FLiBe Molten Salts with Robust Neural Network Interatomic Potential," *ACS Applied Materials & Interfaces*, vol. 13, no. 21, pp. 24 582–24 592, 2021, _eprint: https://doi.org/10.1021/acsami.1c00 DOI: 10.1021/acsami.1c00604. URL: https://doi.org/10.1021/acsami.1c00604.

[14] S. T. Lam, Q.-J. Li, J. Mailoa, C. Forsberg, R. Ballinger, and J. Li, "The impact of hydrogen valence on its bonding and transport in molten fluoride salts," *J. Mater. Chem. A*, vol. 9, no. 3, pp. 1784–1794, 2021, Publisher: The Royal Society of Chemistry. DOI: 10.1039/D0TA10576G. URL: http://dx.doi.org/10.1039/D0TA10576G.

[15] R. Nishiumi, S. Fukada, A. Nakamura, and K. Katayama, "Hydrogen permeation through Flinabe fluoride molten salts for blanket candidates," *Fusion Engineering and Design*, vol. 109-111, pp. 1663–1668, 2016, ISSN: 0920-3796. DOI: https://doi.org/10.1016/j.fusengdes.2015.10.035. URL: https://www.sciencedirect.com/science/article/pii/S0920379615303227.

[16] R. Delaporte-Mathurin, T. Fuerst, and J. Dark, *RemDelaporteMathurin/h-transport-materials: Test release 2*, May 2023. DOI: 10.5281/zenodo.7888448. URL: https://zenodo.org/record/7888448 (visited on 05/08/2023).

[17] K. Dolan, G. Su, G. Zheng, M. Ames, D. Carpenter, and L.-W. Hu, "Experimental Measurement and Multiphysics Simulation of Tritium Transport in Neutron-Irradiated Flibe Salt," en, *Nuclear Technology*, vol. 209, no. 4, pp. 515–531, Apr. 2023, ISSN: 0029-5450, 1943-7471. DOI: 10.1080/00295450.2022.2135933. URL: https://www.tandfonline.com/doi/full/10.1080/00295450.2022.2135933 (visited on 02/21/2024).

[18] G. Ferrero, S. Meschini, and R. Testoni, "A Preliminary CFD and Tritium Transport Analysis for ARC Blanket," en, *Fusion Science and Technology*, vol. 78, no. 8, pp. 617–630, Nov. 2022, ISSN: 1536-1055, 1943-7641. DOI: 10.1080/15361055.2022.2096365. URL: https://www.tandfonline.com/doi/full/10.1080/15361055.2022.2096365 (visited on 11/07/2023).

[19] S. E. Ferry, K. B. Woller, E. E. Peterson, C. Sorensen, and D. G. Whyte, "The LIBRA Experiment: Investigating Robust Tritium Accountancy in Molten FLiBe Exposed to a D-T Fusion Neutron Spectrum," en, *Fusion Science and Technology*, vol. 79, no. 1, pp. 13–35, Jan. 2023, ISSN: 1536-1055, 1943-7641. DOI: 10.1080/15361055.2022.2078136. URL: https://www.tandfonline.com/doi/full/10.1080/15361055.2022.2078136 (visited on 09/01/2023).

[20] R. Delaporte-Mathurin, N. Golesa, J. Ball, *et al.*, "Advancing tritium self-sufficiency in fusion power plants: Insights from the baby experiment," *Preprint submitted to Nuclear Fusion*, 2024, Corresponding author: remidm@mit.edu.

[21] ScienceDirect. "Sherwood number." (), URL: https://www.sciencedirect.com/topics/chemistry/sherwood-number#:~:text=Sherwood%20number%20represents%20the%20ratio,D%20is%20the%20diffusion%20coefficient.

[22] A. Barletta, "The Boussinesq approximation for buoyant flows," *Mechanics Research Communications*, vol. 124, p. 103 939, 2022, ISSN: 0093-6413. DOI: https://doi.org/10.1016/j.mechrescom.2022.103939. URL: https://www.sciencedirect.com/science/article/pii/S0093641322000842.

[23] O. C. Zienkiewicz, R. L. Taylor, and J. Z. Zhu, *The finite element method: its basis and fundamentals*. Elsevier, 2005.

[24] FEniCS Community, *FEniCS project*, https://fenicsproject.org/, Accessed: April 29, 2024.

[25] R. Delaporte-Mathurin, J. Dark, G. Ferrero, E. A. Hodille, V. Kulagin, and S. Meschini, "FESTIM: An open-source code for hydrogen transport simulations," *International Journal of Hydrogen Energy*, vol. 63, pp. 786–802, 2024, ISSN: 0360-3199. DOI: https://doi.org/10.1016/j.ijhydene.2024.03.184. URL: https://www.sciencedirect.com/science/article/pii/S0360319924010218.

[26] Salome Platform, *Salome - the open-source integration platform for numerical simulation*, https://www.salome-platform.org/, Accessed: April 29, 2024.

[27] S. Cantor, "Physical properties of molten-salt reactor fuel, coolant, and flush salts.," Oak Ridge National Lab.(ORNL), Oak Ridge, TN (United States), Tech. Rep., 1968.

[28] R. R. Romatoski and L. W. Hu, "Fluoride salt coolant properties for nuclear reactor applications: A review," *Annals of Nuclear Energy*, vol. 109, pp. 635–647, 2017, ISSN: 0306-4549. DOI: https://doi.org/10.1016/j.anucene.2017.05.036. URL: https://www.sciencedirect.com/science/article/pii/S0306454917301391.

[29] P. Gierszowski, B. Mikic, and N. Todreas, "Property correlations for lithium, sodium, helium, flibe and water in fusion reactor applications," 1980.

[30] S. Cohen and T. Jones, "Viscosity measurements on molten fluoride mixtures," Oak Ridge National Lab.(ORNL), Oak Ridge, TN (United States), Tech. Rep., 1957.

[31] G. J. Janz, F. W. Dampier, G. R. Lakshminarayanan, P. K. Lorenz, and R. P. Tomkins, "Molten salts: Volume i. electrical conductance, density, and viscosity data.," Jan. 1968. URL: https://www.osti.gov/biblio/4162378.

[32] M. R. Zaghloul, "A consistent model for the equilibrium thermodynamic functions of partially ionized flibe plasma with Coulomb corrections," *Physics of Plasmas*, vol. 10, no. 2, pp. 527–538, Feb. 2003, _eprint: https://pubs.aip.org/aip/pop/article-pdf/10/2/527/19321589/ ISSN: 1070-664X. DOI: 10.1063/1.1533067. URL: https://doi.org/10.1063/1.1533067.

[33] V. V. Ignat'ev, A. V. Merzlyakov, V. G. Subbotin, A. V. Panov, and Y. V. Golovatov, "Experimental investigation of the physical properties of salt melts containing sodium and lithium fluorides and beryllium difluoride," en, *Atomic Energy*, vol. 101, no. 5, pp. 822–829, Nov. 2006, ISSN: 1063-4258, 1573-8205. DOI: 10.1007/s10512-006-0175-4. URL: http://link.springer.com/10.1007/s10512-006-0175-4 (visited on 01/23/2024).

[34] D. F. Williams, "Assessment of candidate molten salt coolants for the advanced high temperature reactor (ahtr)," Mar. 2006. DOI: 10.2172/885975. URL: https://www.osti.gov/biblio/885975.

[35] R. Vidrio, S. Mastromarino, E. Still, L. Chapdelaine, and R. O. Scarlat, "Density and Thermal Expansivity of Molten 2LiF-BeF2 (FLiBe): Measurements and Uncertainty Quantification," *Journal of Chemical & Engineering Data*, vol. 67, no. 12, pp. 3517–3531, 2022, _eprint: https://doi.org/10.1021/acs.jced.2c00212. DOI: 10.1021/acs.jced.2c00212. URL: https://doi.org/10.1021/acs.jced.2c00212.

[36] L. J. Chapdelaine, "Experimental and computational study of static solidification of molten fluoride salts for reactor coolant application," Ph.D. dissertation, University of Wisconsin–Madison, 2017.